

Failure Modeling of SiC/SiC Mini-Composites in Air Oxidizing Environments

Guoqiang Yu^{1,2} · Xiguang Gao^{1,2}  · Yue Chen^{1,2} · Yingdong Song^{1,2,3}

Received: 1 January 2018 / Accepted: 13 February 2018 / Published online: 5 March 2018
© Springer Science+Business Media B.V., part of Springer Nature 2018

Abstract An iterative method was presented for simulation of the failure process of SiC/SiC mini-composites with pyrolytic carbon interphase exposed to air oxidizing environments under a constant load at 900 °C. This method was based on the possibility fracture strength of SiC fibers caused by random defects and the fiber stress distribution in mini-composites. The fiber strength probability model and Monte Carlo simulation were combined to generate the fracture strength along SiC fibers at 900 °C. The influence of fiber arrangement on fiber stress distribution was assessed to simplify the geometry model which was used to calculate the fiber stress distribution in the mini-composites. The failure process of the mini-composites was simulated, and the calculated oxidation life of the mini-composites matches the experimental data well with an error of −9.40%.

Keywords SiC/SiC · Mini-composites · Oxidation · Failure · Modeling

1 Introduction

Relatively high strength, high temperature capability, light weight and good corrosion resistance make the silicon carbide fiber reinforced silicon carbide matrix composites (SiC/SiC) for

✉ Xiguang Gao
gaoxiguang@nuaa.edu.cn

✉ Yingdong Song
ydsong@nuaa.edu.cn

¹ Key Laboratory of Aero-engine Thermal Environment and Structure, Ministry of Industry and Information Technology, College of Energy and Power Engineering, Nanjing University of Aeronautics and Astronautics, Nanjing 210016, People's Republic of China

² Jiangsu Province Key Laboratory of Aerospace Power System, College of Energy and Power Engineering, Nanjing University of Aeronautics and Astronautics, Nanjing 210016, People's Republic of China

³ State Key Laboratory of Mechanics and Control of Mechanical Structures, Nanjing University of Aeronautics and Astronautics, Nanjing 210016, People's Republic of China

use in high temperature environments [1–3]. These applications mainly include combustor liners, nozzles, thrusters, etc. which would be constantly loaded in high temperature oxidizing environments for a long time. In SiC/SiC composites with carbon interphase layers, the silicon carbide fiber and matrix have a better resistance to oxidation. However, the carbon interphase between the fiber and matrix is highly sensitive to oxidation in air at high temperatures which alters the performances and the load-carrying capability of the material [4–7]. So it is of great importance to study the mechanisms and effects of the oxidation induced behavior in order to apply SiC/SiC structures in severe service conditions.

The oxidation behavior of SiC/SiC composites with carbon interphase layers has been studied experimentally and numerically. The experimental work mainly focused on the oxidation mechanisms in different situations. Filipuzzi, L. et al. [8] investigated the influence of temperature and carbon interphase thickness on the oxidation of SiC/SiC, and they found three characteristic phenomena during oxidation. Pasquier, S. et al. [7] found that the multi-layered interphases were capable of improving the oxidation resistance of SiC/SiC. The oxidation behavior of SiC/SiC composites in air and combustion environment were investigated and compared by Cheng, L. F. et al. [9]. Their work indicated that due to the protection of silica, the oxidation process decelerated in combustion environment. The parabolic reaction kinetics of carbon interphase which was useful in numerical modeling was studied by Kleykamp et al. [10] and Al Nasiri, N. et al. [11]. However, compared with the experimental work, only a few work had been done to study the numerical modeling method of oxidized SiC/SiC composites. Filipuzzi, L. et al. [12] developed an axisymmetric fiber/interphase/matrix model considering the geometry change, the mass transfers and the chemical reactions. This model was capable to calculate the lengths of carbon interphase consumed by oxidation. Xu, W. et al. [13] proposed an analytical models incorporating the combined kinetic effects of oxide growth and viscous flow. The model predicted the oxidation life of SiC/SiC composites. However, this model was developed for the SiC/SiC composites with boron nitride interphase. Therefore, the numerical modeling study for SiC/SiC composites with carbon interphase was still insufficient which would largely hinder the application of SiC/SiC components.

Motivated by such situation, the aim of this paper is to develop a numerical model for SiC/SiC mini-composites with pyrolytic carbon (PyC) interphase to simulate the failure process induced by interphase oxidation under a constant tensile load in air at high temperatures. In this paper, the tensile strength distribution along axial direction of SiC fibers at high temperature was simulated by fiber strength probability model and Monte Carlo method. The finite element method was adopted to evaluate the influence of fiber arrangement on fiber stress distribution. Then a simplified model was developed based on the evaluation and was integrated with the fiber tensile strength distribution in an iterative algorithm to model the failure process of SiC/SiC mini-composites with PyC interphase. Finally, the oxidation life of the SiC/SiC mini-composites under a constant tensile load in air at 900 °C was obtained based on the method developed in this paper which agrees well with the experiment results.

2 Material and Experiment

2.1 Material Description

The mini-composites used in this paper is composed of silicon carbide fibers (1 K tow, CERAFIL Ltd., China) reinforced in chemical vapor infiltration (CVI) silicon carbide

matrices. A PyC layer with a thickness of $1.5\ \mu\text{m}$ is deposited on the surface of SiC fibers before the densification of the silicon carbide matrices. The detailed CVI process parameters can be found in [14–16]. The radius of SiC fiber is $\sim 6\ \mu\text{m}$. The fiber volume fraction of the SiC/SiC mini-composites is $\sim 16.6\%$. The density of the SiC/SiC mini-composites is $\sim 3.1\ \text{g/cm}^3$.

2.2 Oxidation Failure Experiment

The configuration of the experiment appliance is illustrated in Fig. 1. The upper connection and the lower connection were made of aluminum alloy. The upper connection was used to link the fixed end with the rest parts of the experiment appliance. The lower connection was designed to mount the weight to load the specimen. The high temperature alloy fixture was made of GH4169. The connections and the fixtures were connected by alloy pins. The high temperature alloy fixture has two symmetrical parts to grip the specimen. High temperature alloy bolts were adopted to compress the two parts of the fixture. The Al_2O_3 tubes were utilized to avoid the mini-composites specimen from being crushed. In this paper, the high temperature resistant adhesive was applied to glue the tubes to the specimen. The dimension of the specimen is shown in Fig. 1 as well.

During the oxidation failure experiment, the weight was hanged on the lower connection through a hole to load the specimen after the temperature of the furnace reaches to $900\ ^\circ\text{C}$. The experiment results shown that the oxidation life of SiC/SiC mini-composites used in this paper is about 6.70 h under a 6 kg tensile load in air at $900\ ^\circ\text{C}$.

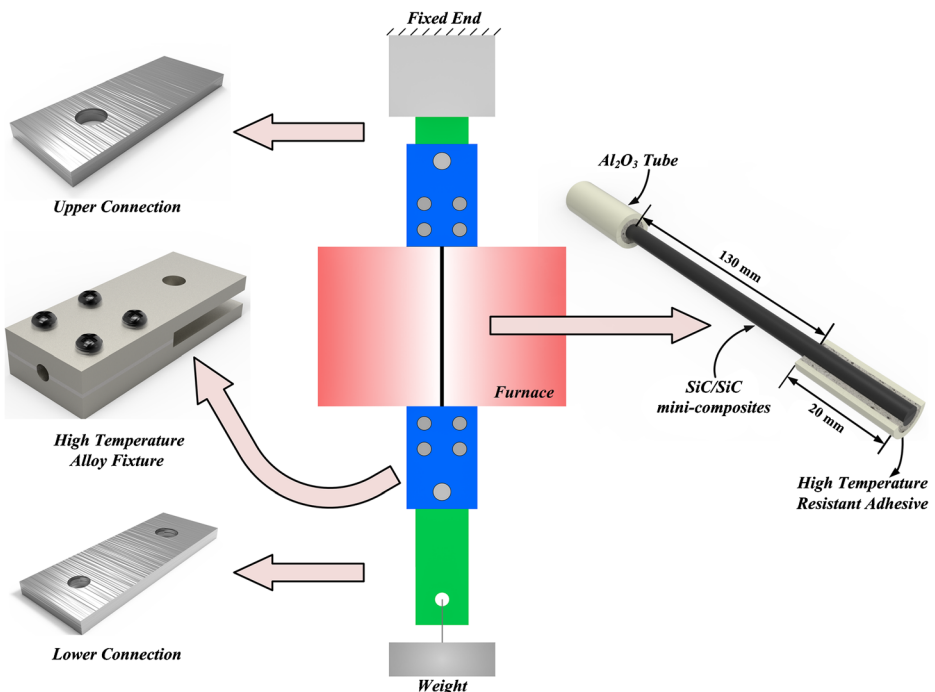


Fig. 1 Schematic diagram of the oxidation test appliance in air for mini-composites

3 Modeling and Analysis

3.1 Axial Tensile Strength Distribution Simulation of SiC Fibers

The tensile strength of mini-composites is primarily determined by the strength of fibers. So the strength model of SiC fibers plays an important role in modeling the failure of SiC/SiC mini-composites. The tensile strength distribution of SiC fibers at room temperature is shown in Fig. 2 [17]. The tensile strength disparities are mainly caused by different defects along fibers such as micro cracks, voids, inclusions, disordered SiC crystal arrangement, etc. Moreover, due to the damages induced by preparation process and mechanical performance degradation caused by high temperature, the in situ strength of SiC fibers in mini-composites is different from the original SiC fibers. The effects of preparation process and high temperature are assumed to change the strength values only without changing the strength distribution form of SiC fibers [18]. Thus the in situ tensile strength of SiC fibers can be estimated by the following equation,

$$\sigma_{in\ situ} = \beta_1 \beta_2 \sigma_{ori} \quad (1)$$

where $\sigma_{in\ situ}$ represents the in situ tensile strength of SiC fibers in mini-composites at high temperatures, σ_{ori} denotes the tensile strength of SiC fibers at room temperature, β_1 and β_2 are coefficients represent the effects of preparation process and high temperature degradation respectively. β_1 is defined as,

$$\beta_1 = \bar{\sigma}_{HT} / \bar{\sigma}_{RT} \quad (2)$$

where $\bar{\sigma}_{HT}$ and $\bar{\sigma}_{RT}$ are the average tensile strength of SiC fibers at high temperature and room temperature respectively. The average tensile strength of SiC fibers at room temperature is 1.29 GPa, and the average tensile strength of SiC fibers at high temperature (900 °C) is 1.02 GPa [17]. It was reported that the mechanical properties of SiC fibers decrease by 50% after the preparation process of mini-composites [19], that is, the value of β_2 is 0.5.

In this paper, the fiber strength probability model (FSPM) is utilized to calculate the fiber failure probabilities (X. Gao, S. Zhang and Y. Song, In situ strength model for continuous fibers and multi-scale modeling the fracture of C/SiC minicomposite under tensile loading, manuscript submitted). The FSPM classifies defects based on in situ strength of fibers and assumes that defects appear randomly along fibers. Based on the framework of FSPM, the fiber failure probability caused by the j^{th} defect can be expressed as,

$$P_j = 1 - [1 - P(A_j)]^{\Delta l / L} \quad (3)$$

where $P(A_j)$ is the probability of j^{th} defect in SiC fiber with a length of L , Δl denotes the length of each discrete SiC fiber elements.

$P(A_j)$ can be estimated by the following equations,

$$P(A_1) = P(B_1) \quad (4)$$

$$P(A_j) = P(B_j) / \prod_{k=1}^{j-1} [1 - P(A_k)] \quad (j = 1, 2, \dots, n) \quad (5)$$

$$P(B_j) = c_j / N_L \quad (j = 1, 2, \dots, n) \quad (6)$$

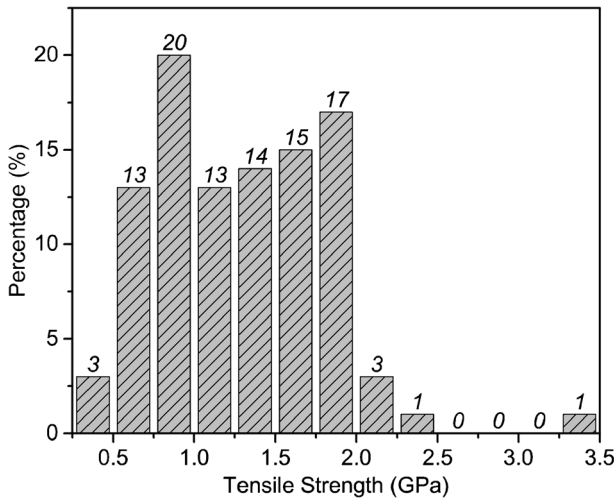


Fig. 2 Tensile strength distribution of SiC fibers at room temperature

where N_L is the total number of fibers in SiC/SiC mini-composites with a length of L , c_j is the number of fibers with a tensile strength of σ_j .

In this paper, $P(B_j)$ can be obtained directly based on the data showed in Fig. 2. The length of SiC fiber is set to 200 mm which is consistent with the SiC fiber tensile strength distribution tests. The length of each discrete SiC fiber elements is set to 25 μm .

The tensile strength of every SiC fiber element was determined by critical possibility factor η and P_j in this paper. The critical possibility factor η range from 0 to 1 and was derived from Monte Carlo simulation. If η is less than or equal to P_j , the j^{th} defect appears in SiC fiber element Δl . The strength of SiC fiber element is expressed as $\sigma_{\Delta l}$ and is equal to the minimum strength caused by certain defects in the SiC fiber element. The tensile strength distribution of SiC fibers can be achieved by repeating the above procedures in different Δl along the fiber

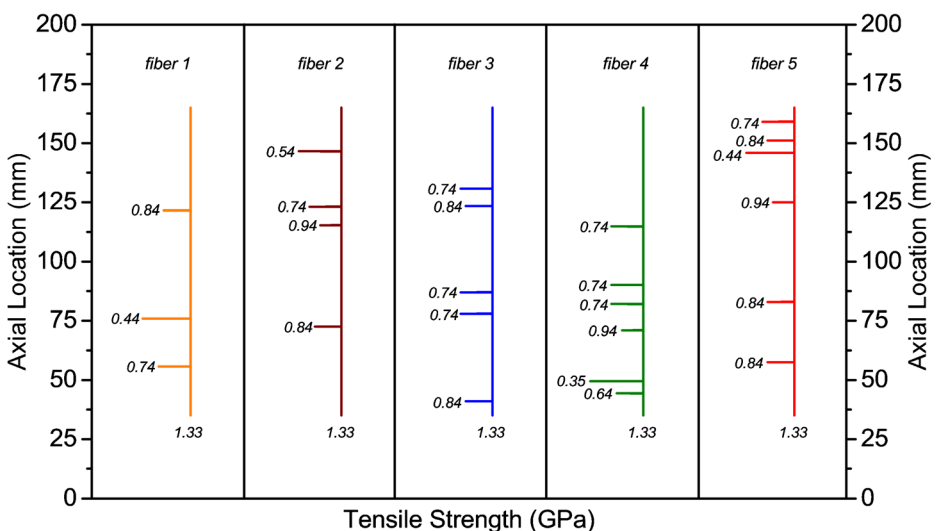


Fig. 3 Examples of simulated SiC fiber axial tensile strength distribution at 900 °C

direction. Examples of the simulated results are illustrated in Fig. 3. The results show that most SiC fiber elements have a relatively high strength while some parts of SiC fiber elements have a very low strength. The minimum strength among all the elements in the same SiC fiber is the failure strength of the fiber. In real SiC fibers, most defects have little impact on the strength of SiC fibers except some serious defects which will lead to a low fracture stress of SiC fibers. Therefore, the results correspond well with the reality.

3.2 Effects of Fiber Arrangement on Fiber Stress Distribution

Fibers in actual mini-composites are not strictly parallel to the axial direction which would lead to a non-uniform stress distribution along fibers. Furthermore, the non-uniform stress distribution will cause uneven oxidation process in mini-composites. So if the stress distribution is severe non-uniform, the actual fiber arrangement must be considered in modeling process. However, modeling the actual fiber distribution in mini-composites will increase the workload and computing time largely. Thus, it is important to evaluate the necessity of applying the real fiber distribution in finite element models.

In this paper, a finite element model with real fiber distribution was established. The model contains 15 representative fibers in which 10 fibers are completely parallel to the axial direction, 3 fibers are oblique and 2 fibers are bend (see Fig. 4). The representative geometrical model of SiC/SiC mini-composites with the mentioned fiber arrangement and a prepared matrix crack is shown in Fig. 5. The axial length of the model is equal to the distance between two adjacent matrix cracks (500 μm). The oxidation length of PyC interphase in the model is 35 μm . The fiber radius is 6 μm and the surface is deposited with a PyC interphase with a thickness of 1.5 μm uniformly.

It is hard to measure matrix crack opening distance directly under high temperature environment, so the matrix crack opening distance showed in Fig. 5 was calculated by the following equation [20],

$$L_{HT}(T) = L_{RT} \left(1 - \frac{T}{T_0} \right) \quad (7)$$

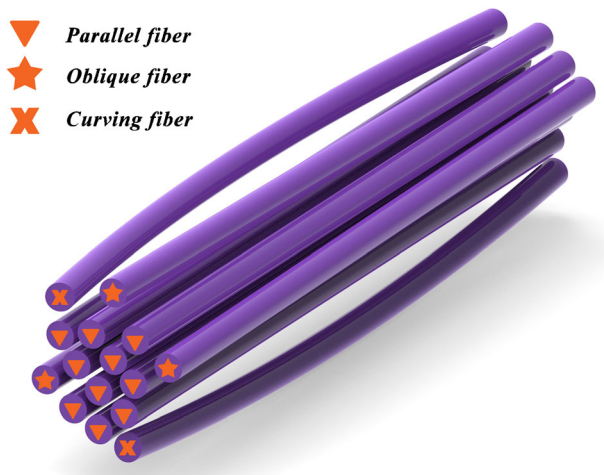


Fig. 4 Representative fiber distribution in mini-composites

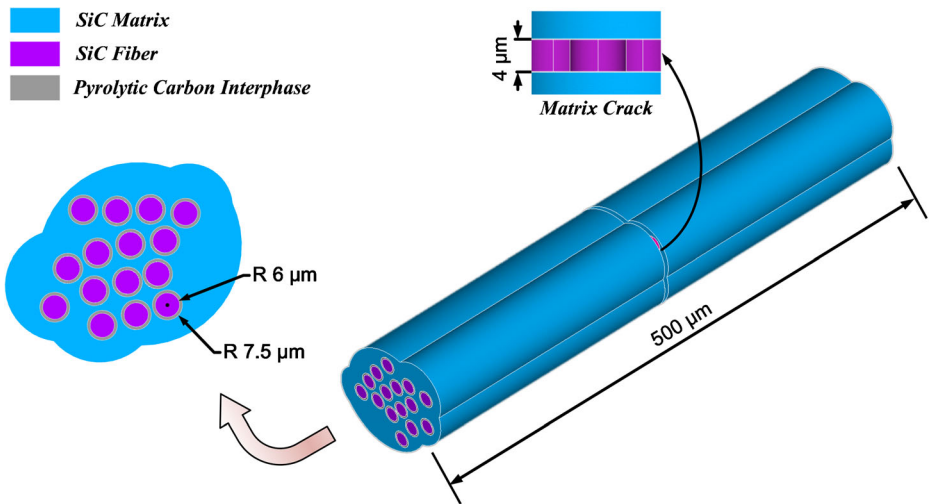


Fig. 5 Representative geometrical model of SiC/SiC mini-composites

where $L_{HT}(T)$ is the matrix crack opening distance at temperature T , L_{RT} represents the matrix crack opening distance at room temperature. T_0 denotes the matrix crack closure temperature. In this paper L_{RT} is 16 μm , T_0 is 1200 $^\circ\text{C}$. By Eq. (7), the matrix crack opening distance at 900 $^\circ\text{C}$ is 4 μm .

The representative model of SiC/SiC mini-composites was loaded with a constant stress of 108 MPa which corresponds with the experiment load 6 kg. The average tensile stress of fiber cross sections was used to represent the equivalent stress of the cross section. The equivalent stresses along axial direction of mini-composites were extracted and plotted in Fig. 6.

Figure 6 shows that the 15 fibers have the same axial equivalent stress distribution pattern. However, the axial equivalent stress in the same axial location varies between

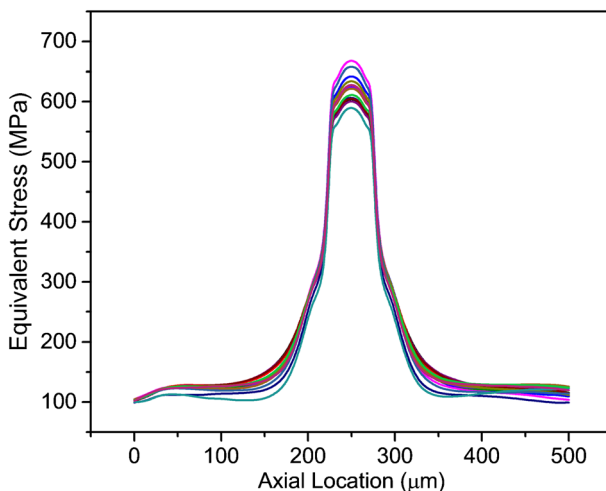


Fig. 6 Axial equivalent stress distribution of the 15 fibers in the representative model

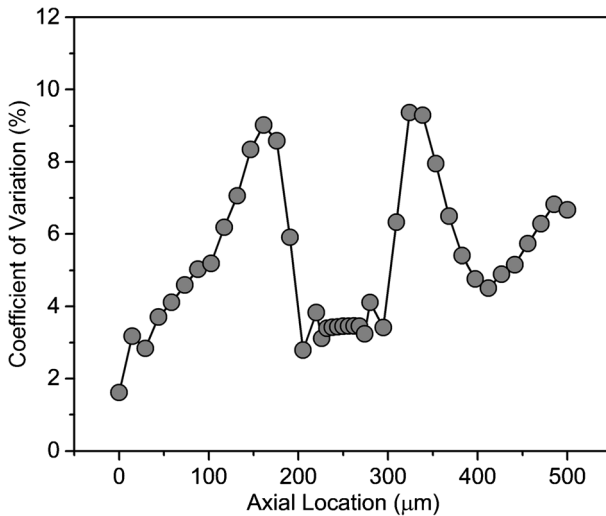


Fig. 7 Coefficient of variation of fiber axial equivalent stress

different fibers due to the uneven fiber arrangement. In addition, the fiber axial equivalent stress increases steeply on account of matrix cracks and PyC interphase oxidation. The maximum axial equivalent stress appears in the middle of the model which is consistent with the reality.

To assess the heterogeneous stresses in different fibers quantitatively, the coefficient of variation was employed. The expression of coefficient of variation (CV) was given as follows,

$$CV = \sqrt{\frac{1}{n} \sum_{i=1}^n \left(\sigma_i - \frac{1}{n} \sum_{i=1}^n \sigma_i \right)^2} / \frac{1}{n} \sum_{i=1}^n \sigma_i \quad (8)$$

where σ_i is the axial equivalent stress in fiber i , n is the amount of fibers.

Figure 7 depicts the CV curve of fiber axial equivalent stress in the representative model. It can be found that every data point is lower than 10% which indicates that the actual uneven fiber arrangement does not introduce much non-uniformity. Therefore, the uneven fiber arrangement can be neglected. The simplified finite element model was developed in the next section.

3.3 Simplified Fiber Stress Distribution Calculation Model

As discussed in the previous section, the irregular fiber arrangement in real mini-composites has limited effects on the fiber stress distribution. Hence, a simplified finite element model contains single SiC fiber was developed in this section to reduce the modeling complexity and computing cost. The schematic diagram of the simplified geometry model was illustrated in Fig. 8.

In the simplified model, the interfacial thickness and the fiber radius are the same as the representative geometrical model of SiC/SiC mini-composites illustrated in Fig. 5. The thickness of silicon carbide matrix was calculated by volume fraction. L_{SM} is the length of

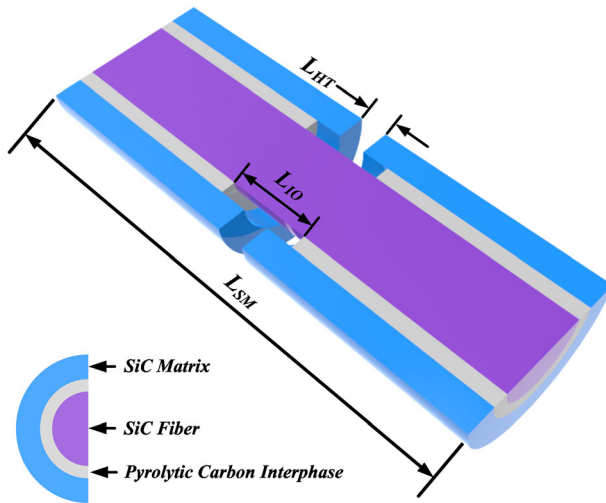


Fig. 8 Profile diagram of the simplified geometry model

the simplified model which is equal to the space between two neighboring matrix cracks. L_{HT} is the matrix crack opening distance at temperature T which can be obtained by Eq. (7). The PyC interphase was exposed to high temperature air due to matrix cracks. Thus the interphase around the matrix crack disappears gradually due to oxidation. The PyC interphase oxidation length is denoted as L_{IO} . The relationship between oxidation length and time can be expressed as [21],

$$L_{IO} = k_0 \exp(-E_a^I / RT) \frac{P_{air} f_{O_2} M_C^I}{RT \rho_C^I} t \tag{9}$$

where R is the gas constant, T is the oxidation temperature, P_{air} denotes the pressure of high temperature air, f_{O_2} is the fraction of oxygen in the air, k_0 represents the exponential factor, E_a^I is the activation energy for the oxidation reaction, t indicates the oxidation time, ρ_C^I and M_C^I are the density and molar mass of the PyC interphase respectively. The oxidation dynamic parameters are listed in Table 1.

The numerical results (see Fig. 9) shows that the simplified model gives the same fiber axial stress distribution compared well with the representative SiC/SiC mini-composites model which validated the equivalency of simplification. Furthermore, Fig. 9 indicates that the growth of oxidation length enlarged the overall stress level of the fibers which would boost the failure possibility of the fibers.

Table 1 Oxidation dynamic parameters

E_a^I (kJ/mol)	ρ_C^I (kg/m ³)	M_C^I (kg/mol)	k_0 (s ⁻¹)	P_{air} (Pa)	f_{O_2}
118.3	2267	0.012	0.23	101,300	0.21

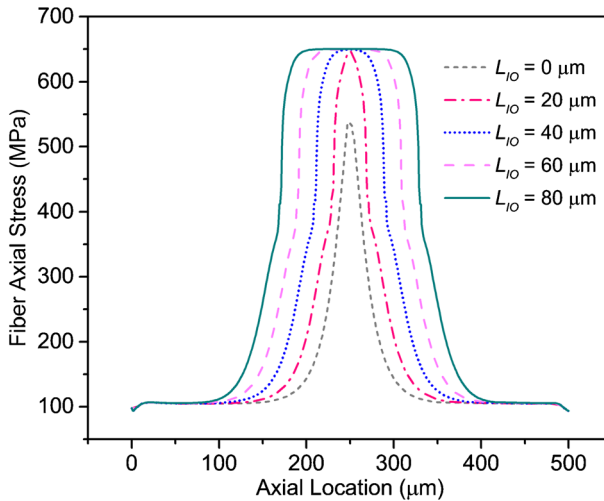


Fig. 9 Fiber axial stress distribution in different oxidation length

3.4 Failure Simulation Algorithm for SiC/SiC Mini-Composites with PyC Interphase

In mini-composites, the strength distribution varies among different fibers. The fibers with low fracture strength fail first and lead to stress re-distribution among residual fibers. To be exact, the failed fibers increase the stress levels of intact fibers under a constant external force. After the stress re-distribution, the residual fibers which satisfy the failure condition fail subsequently. The new failed fibers lead to another stress re-distribution process. The above process repeats till all fibers in mini-composites failed. In this paper, the failure process of mini-composites was simulated by integrating simplified fiber stress distribution calculation model with the fiber tensile strength distribution simulation method in an iterative algorithm. The failure simulation procedure is shown in Fig. 10.

In this simulation framework, the PyC interphase oxidation length L_{IO} was obtained firstly by the given oxidation time t and Eq. (9). The applied stress on the simplified finite element model was the nominal stress caused by fiber stress re-distribution effect. The fiber axial stress distribution was obtained from the finite element results subsequently. The applied nominal stress under a constant external force was expressed as,

$$\sigma_n = \sigma_0 \frac{1000}{1000-m} \quad (10)$$

where σ_0 is the initial external load and m is the number of failed fibers.

The fiber strength distribution of the 1000 fibers in the mini-composites was generated by fiber strength probability model and Monte Carlo method. In the simulation procedure, the fiber axial stress distribution was compared with the fiber strength distribution point-by-point. If the fiber fracture strength is lower than the fiber axial stress, it means that the fiber ruptures at that location. Otherwise, no failure appears. Fig. 11 shows two examples of the comparison results, Fig. 11a is the non-fracture situation and Fig. 11b is the case of fiber fracture.

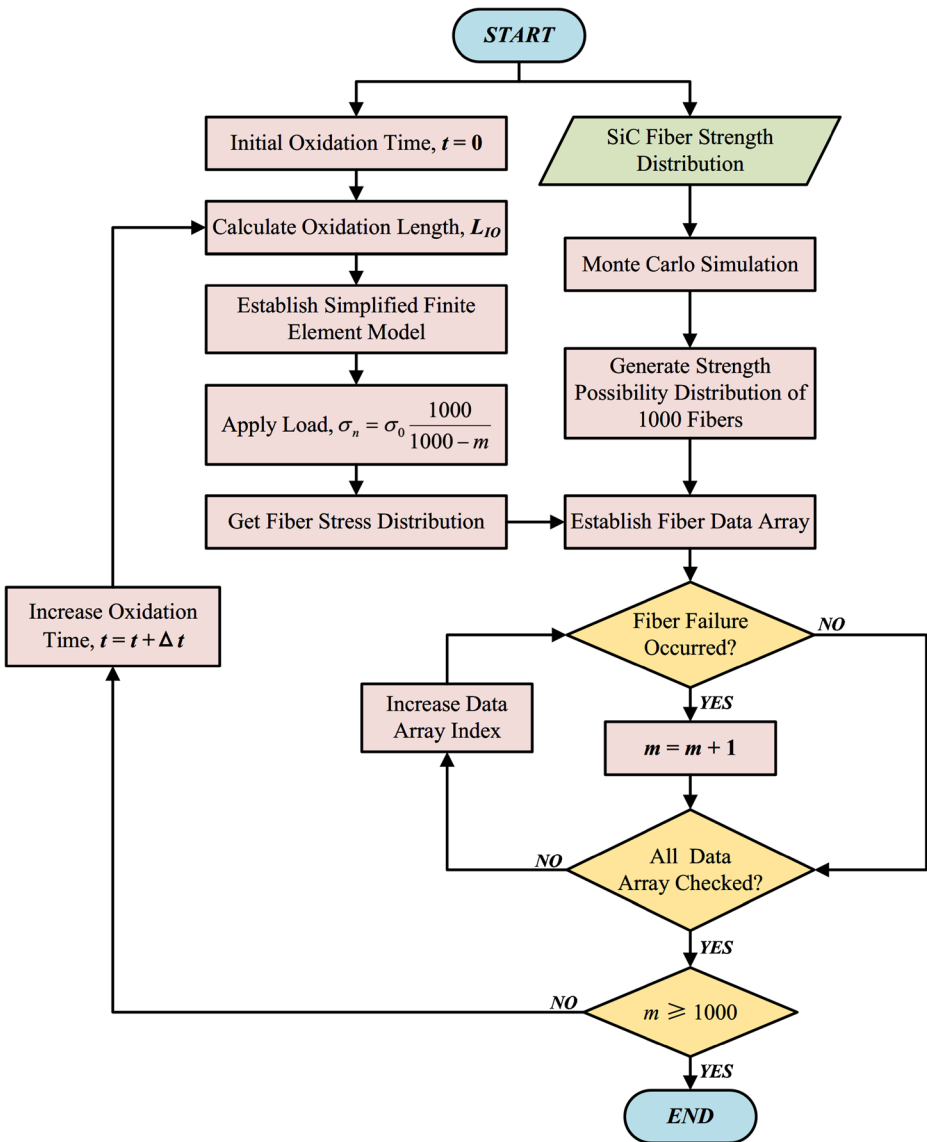


Fig. 10 Flowchart of failure simulation algorithm for SiC/SiC mini-composites with PyC interphase

Fig. 12 depicts the enlarged view of the fiber fracture location to give a more clearly view of the results.

The parameter m was used to record the amount of failed fibers. If $m < 1000$ in one oxidation step, it indicates that the mini-composites do not fail. Thus the process continues to move to the next oxidation step that is $t = t + \Delta t$. If $m \geq 1000$, it means that all fibers ruptured at this step, that is, the mini-composites failed. Besides, the final oxidation time t is regarded as the oxidation life of the mini-composites under the given load and temperature.

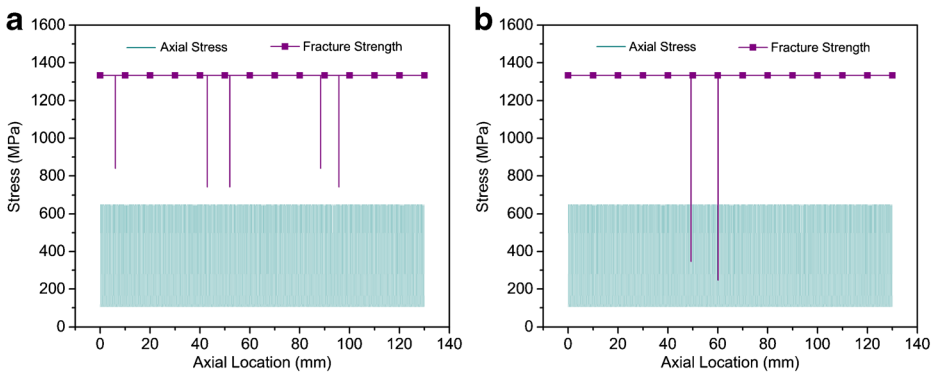


Fig. 11 Examples of simulated results: **a** non-fracture situation, **b** fiber fracture situation

The simulated failure process is illustrated in Fig. 13. It shows that the fiber failure amount increases linearly at the beginning. As the oxidation process goes on, the fiber failure process speeds up dramatically. All of the 1000 fibers failed completely after 6.07 h at a 6 kg tensile load in air at 900 °C. The simulated oxidation life of the SiC/SiC mini-composites is 9.40% smaller than that of the experiment results (6.70 h). Therefore, the method developed in this paper is capable of simulating the failure process of SiC/SiC mini-composites under a constant tensile load in air oxidizing environments at high temperatures with an acceptable accuracy.

4 Conclusions

In the present study, the SiC fiber tensile strength distribution in SiC/SiC mini-composites was obtained by the fiber strength probability model and Monte Carlo simulation. The results correspond well with the reality.

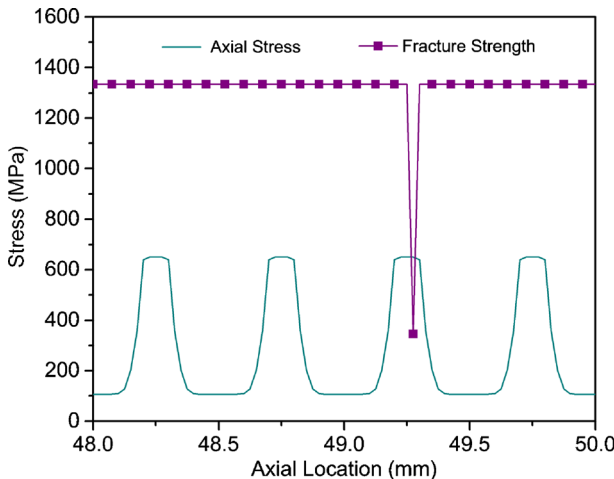


Fig. 12 Enlarged view of fiber fracture location

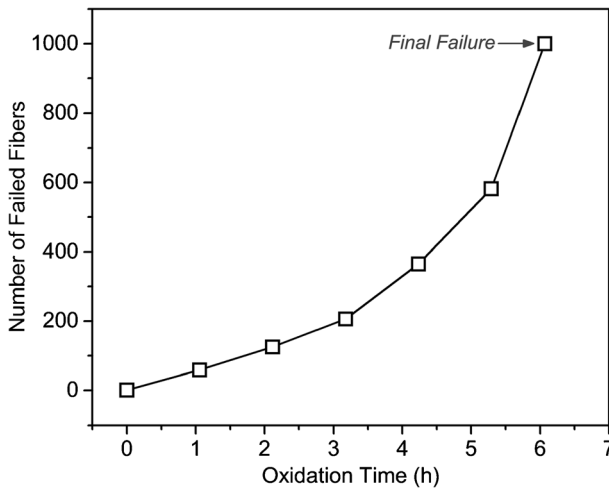


Fig. 13 Failure process of SiC/SiC mini-composites

The numerical results of the representative mini-composites model containing real fiber arrangement shows that the effects of fiber arrangement on fiber stress distribution can be neglected. The simplified fiber stress calculation model is feasible to generate the reasonable fiber axial stress distribution.

By incorporating the simplified fiber stress distribution calculation model and fiber tensile strength distribution in the proposed iterative algorithm, the failure process of SiC/SiC mini-composites with PyC interphase under a constant load in air oxidizing environments at high temperatures was simulated successfully. The numerical results illustrated the failure rate change during the failure process. Moreover, the method gives a very reasonable results with an error of -9.40% compared with the experimental data.

Acknowledgments This work was supported by the National Key Research and Development Program of China (grant number 2017YFB0703200); the National Natural Science Foundation of China [grant numbers 51575261, 51675266]; and the Priority Academic Program Development of Jiangsu Higher Education Institutions.

References

- Naslain, R.: Design, preparation and properties of non-oxide CMCs for application in engines and nuclear reactors: an overview. *Compos. Sci. Technol.* **64**(2), 155–170 (2004)
- Ohnabe, H., Masaki, S., Onozuka, M., Miyahara, K., Sasa, T.: Potential application of ceramic matrix composites to aero-engine components. *Compos. A: Appl. Sci. Manuf.* **30**(4), 489–496 (1999)
- Staeher, J.M., Zawada, L.P.: Performance of four ceramic-matrix composite divergent flap inserts following ground testing on an F110 turbofan engine. *J. Am. Ceram. Soc.* **83**(7), 2010 (1727–1738)
- Gowayed, Y., Abouzeida, E., Smyth, I., Ojard, G., Ahmad, J., Santhosh, U., Jefferson, G.: The role of oxidation in time-dependent response of ceramic-matrix composites. *Compos. Part B Eng.* **76**, 20–30 (2015)
- Casas, L., Martínez-Esnaola, J.M.: Modelling the effect of oxidation on the creep behaviour of fibre-reinforced ceramic matrix composites. *Acta Mater.* **51**(13), 3745–3757 (2003)
- Jacques, S., Lopez-Marure, A., Vincent, C., Vincent, H., Bouix, J.: SiC/SiC minicomposites with structure-graded BN interphases. *J. Eur. Ceram. Soc.* **20**(12), 1929–1938 (2000)
- Pasquier, S., Lamon, J., Naslain, R.: Tensile static fatigue of 2D SiC/SiC composites with multilayered (PyC-SiC)(n) interphases at high temperatures in oxidizing atmosphere. *Compos. A: Appl. Sci. Manuf.* **29**(9–10), 1157–1164 (1998)

8. Filipuzzi, L., Camus, G., Naslain, R., Thebault, J.: Oxidation mechanisms and kinetics of 1D-SiC/C/SiC composite materials: I, An experimental approach. *J. Am. Ceram. Soc.* **77**(2), 459–466 (2010)
9. Cheng, L.F., Xu, Y.D., Zhang, L.T., Yin, X.W.: Oxidation behavior of three-dimensional SiC/SiC composites in air and combustion environment. *Compos. A: Appl. Sci. Manuf.* **31**(9), 1015–1020 (2000)
10. Kleykamp, H., Schauer, V., Skokan, A.: Oxidation behaviour of SiC fibre reinforced SiC. *J. Nucl. Mater.* **227**(95), 130–137 (1995)
11. Al Nasiri, N., Patra, N., Ni, N., Jayaseelan, D.D., Lee, W.E.: Oxidation behaviour of SiC/SiC ceramic matrix composites in air. *J. Eur. Ceram. Soc.* **36**(14), 3293–3302 (2016)
12. Filipuzzi, L., Naslain, R.: Oxidation mechanisms and kinetics of 1D-SiC/C/SiC composite materials: II, modeling. *J. Am. Ceram. Soc.* **77**(2), 467–480 (2010)
13. Xu, W., Zok, F.W., McMeeking, R.M.: Model of oxidation-induced fiber fracture in SiC/SiC composites. *J. Am. Ceram. Soc.* **97**(11), 3676–3683 (2014)
14. Yu, G., Gao, X., Song, Y.: Experimental investigation of the in-plane shear behavior on needled C/SiC composites using digital image correlation. *J. Ceram. Sci. Technol.* **7**(4), 387–396 (2016)
15. Tang, S., Deng, J., Wang, S., Liu, W., Yang, K.: Ablation behaviors of ultra-high temperature ceramic composites. *Mater. Sci. Eng. A.* **465**(1–2), 1–7 (2007)
16. Tang, S., Deng, J., Du, H., Liu, W., Yang, K.: Fabrication and microstructure of C/SiC composites using a novel Heaterless chemical vapor infiltration technique. *J. Am. Ceram. Soc.* **88**(11), 3253–3255 (2005)
17. Simon, G., Bunsell, A.R.: Mechanical and structural characterization of the Nicalon silicon carbide fibre. *J. Mater. Sci.* **19**(11), 3649–3657 (1984)
18. Jiang, D., Wang, Y., Zhou, Y., Xia, Y.: In-situ strength of carbon fibers in silicon carbide matrix composites. *Acta Materiae Compositae Sinica.* **18**(3), 67–71 (2001)
19. Guo, S., Kagawa, Y.: Effect of matrix modification on tensile mechanical behavior of Tyranno®; Si-Ti-C-O fiber-reinforced SiC matrix minicomposite at room and elevated temperatures. *J. Eur. Ceram. Soc.* **24**(10–11), 3261–3269 (2004)
20. Naslain, R., Guette, A., Rebillat, F., Gallet, S.L., Lamouroux, F., Filipuzzi, L., Louchet, C.: Oxidation mechanisms and kinetics of SiC-matrix composites and their constituents. *J. Mater. Sci.* **39**(24), 7303–7316 (2004)
21. Xu, Y., Zhang, P., Lu, H., Zhang, W.: Numerical modeling of oxidized C/SiC microcomposite in air oxidizing environments below 800 °C: microstructure and mechanical behavior. *J. Eur. Ceram. Soc.* **35**(13), 3401–3409 (2015)